

Nonlinear corrections on the parametrization methods

G.R.Boroun* and B.Rezaei†

Department of Physics, Razi University, Kermanshah 67149, Iran

(Dated: October 11, 2021)

We present non-linear corrections (NLC) to the distribution functions at low values of x and Q^2 using the parametrization $F_2(x, Q^2)$ and $F_L(x, Q^2)$. We use a direct method to extract non-linear corrections to the ratio of structure functions and the reduced cross section in the next-to-next-to-leading order (NNLO) approximation with respect to the parametrization method (PM). Comparison between the non-linear results with the bounds in color dipole model (CDM) and HERA data indicate the consistency of the non-linear behavior of the gluon distribution function at low- x and low- Q^2 . The non-linear longitudinal structure functions are comparable with the H1 Collaboration data in a wide range of Q^2 values. Consequently, the non-linear corrections at NNLO approximation to the reduced cross sections at low and moderate Q^2 values show good agreement with the HERA combined data. These results at low x and low Q^2 can be applied to the LHeC region for analyses of ultra-high-energy processes.

1. Introduction

Based on parton model and perturbative quantum chromodynamics (pQCD), the Dokshitzer-Gribov-Lipatov-Altarelli-Parisi (DGLAP) evolution equations [1] successfully and quantitatively interpret the Q^2 -dependence of parton distribution functions (PDFs). The small- x behavior due to DGLAP equations is driven by input distributions at a starting scale $Q = Q_0$. In recent years several different parametrizations of PDF from a global fits to the available data have been introduced [2-4]. PDF groups, such as Refs.[2,3], analysis HERA data [5] in their global analysis. Recently in Ref.[4] authors presented the parton distribution functions using a wide variety of high-precision Large Hadron Collider (LHC) data in addition to the combined HERA I+II deep-inelastic scattering data set. LHC covered data sample of over 140 fb^{-1} at the 13 TeV run for both ATLAS and CMS collaborations. The CT global analyses [4] explored a broad range of parametric forms for the parton distribution functions at the starting scale, $Q = Q_0$. In CT18 the initial nonperturbative parametrizations are written in the following formal form

$$f_i(x, Q_0) = \alpha_0 x^{\alpha_1 - 1} (1 - x)^{\alpha_2} P_i(y, \alpha_3, \alpha_4, \dots),$$

where the coefficients α_1 and α_2 control the asymptotic behavior of $f_i(x, Q_0)$ in the limits $x \rightarrow 0$ and 1, and P_i is a sum of Bernstein polynomials dependent on $y = f(x)$ which is very flexible across the whole interval $0 < x < 1$. At extremely small of the Bjorken variable x , the pQCD evolution provides a rather singular behavior of the PDFs which strongly violates the Froissart boundary [6]. With

respect to HERA data, some new parametrizations of the proton structure function have been proposed by authors in Refs.[7,8] in a wide range of Q^2 values which are in a full accordance with the Froissart predictions. These parametrizations are relevant in investigations of ultra-high energy processes, such as scattering of cosmic neutrino off hadrons. The importance of ultra-high energies is in explore extreme regions of the (Q^2, x) phase space, where non-accelerator data exist [9]. Studies along energy boost not only confirm HERA investigations but also provide crucial benchmarks for further investigations of the high-energy limit of QCD at the Large Hadron electron Collider (LHeC) [10]. The kinematic extension of the LHeC will allow us to examine the non-linear dynamics at low x [11,12]. The non-linear region is approached when the reaction is mediated by multi-gluon exchange. Indeed the gluon-gluon recombination processes cause that the growth of the gluon density is slowed down at smaller values of x and Q^2 (but still $Q^2 \gg \Lambda_{QCD}^2$) [13,14]. At this region gluon recombination terms, which lead to non-linear corrections to the evolution equations, can become significant. Gluon recombination in deep inelastic and diffractive scattering were published some time ago in Refs.[14] and [15] respectively. The gluon density cannot grow forever because hadronic cross-sections comply with the unitarity bound known as Froissart Bound [6]. Indeed the unitarity (or Froissart bound states) does not grow faster than $\sigma < \pi d^2 \ln^2(s/s_0)$ where d is some typical hadronic scale and s is the Mandelstam variable denoting the square of the total invariant energy of the process. The gluon recombination effects tamed growth of the gluon density towards low x . These effects induce non-linear power corrections to the DGLAP equations. Some studies of the non-linear behavior of PDFs are given in Refs.[16-30] in recent years.

Low x physics at the LHeC and Future Circular Collider hadron-electron (FCC-he) is an area for discovery non-linear effects. This extends the kinematic reach, of

*Electronic address: grboroun@gmail.com; boroun@razi.ac.ir

†brezaei@razi.ac.ir

maximum $Q^2 \simeq 1 \text{ TeV}^2$ and $x \propto Q^2/s \simeq 10^{-5} \dots -6$ for LHeC and 10^{-7} for FCC-he, where parton interaction must to become non-linear. The extended kinematic range of the LHeC provides unique avenues to explore the possible onset of non-linear QCD dynamics at small- x [10,11,12]. In Ref.[31] PDF4LHC15 includes HERA data down to $x \simeq 10^{-4}$ which is successfully described via the DGLAP framework.

The non-linear evolution in high-density QCD is considered in a shock wave color field of the target in Ref.[32]. Authors have considered deeply inelastic scattering at very high energies in the saturation regime and have developed a formalism which allows to evaluate successively the non-linearities in the generalized evolution equation for the dipole densities. In Ref.[33] authors have discussed the results of the analytical and numerical analysis of the non-linear Balitsky-Kovchegov equation. One of the important outcomes of studied in Ref.[33] is the existence of the saturation scale $Q_s(x)$ which is a characteristic scale at which the parton recombination effects become important. The solution to the non-linear equation has the property of the geometric scaling in the regime where $k < Q_s(x)$ whereas in the case when $k > Q_s(x)$ the solution enters the linear regime, where k is the gluon transverse momenta. The phenomenological implications of the parton distribution functions sets with small- x resummation for the longitudinal structure function F_L at HERA have investigated in Ref.[34]. Also a resolution of the incorporating $\ln(1/x)$ -resummation terms into the HERAPDF fits have investigated using the xFitter program. Authors in Ref.[35] have tried to investigate solutions of the non-linear evolution equation in the nonperturbative part of the low x region.

The non-linear terms have been calculated by Gribov-Levin-Ryskin (GLR) and Mueller-Qiu (MQ) in [36]. GLR originally showed how to qualitatively modify the DGLAP gluon evolution equation in order to incorporate effects of gluon recombination, then MQ derived the singlet evolution equation for the conversion of gluon to quarks. The modified evolution equations, due to the fusion of two gluon ladders, denote as the GLR-MQ equations

$$\frac{\partial xg(x, Q^2)}{\partial \ln Q^2} = \frac{\partial xg(x, Q^2)}{\partial \ln Q^2} \Big|_{DGLAP} - \frac{81}{16} \frac{\alpha_s^2(Q^2)}{\mathcal{R}^2 Q^2} \int_{\chi}^1 \frac{dz}{z} \left[\frac{x}{z} g\left(\frac{x}{z}, Q^2\right) \right]^2, \quad (1)$$

and

$$\frac{\partial F_2(x, Q^2)}{\partial \ln Q^2} = \frac{\partial F_2(x, Q^2)}{\partial \ln Q^2} \Big|_{DGLAP} - \frac{5}{18} \frac{27\alpha_s^2(Q^2)}{160\mathcal{R}^2 Q^2} [xg(x, Q^2)]^2, \quad (2)$$

where $g(x, Q^2)$ is the gluon density, $xg(x, Q^2) = G(x, Q^2)$ is the gluon density momentum. Here $\chi = \frac{x}{x_0}$ and x_0 is

the boundary condition that the gluon distribution (i.e., $G(x, Q^2)$) joints smoothly onto the linear region. The correlation length \mathcal{R} determines the size of the non-linear terms. This value depends on how the gluon ladders are coupled to the nucleon or on how the gluons are distributed within the nucleon. The \mathcal{R} is approximately equal to $\simeq 5 \text{ GeV}^{-1}$ if the gluons are populated across the proton and it is equal to $\simeq 2 \text{ GeV}^{-1}$ if the gluons have hotspot like structure. Here the higher dimensional gluon distribution (i.e., higher twist) is assumed to be zero. In the small x region, the saturation scale $Q_s^2(x)$ ($Q_s^2 = Q_0^2(x/x_0)^{-\lambda}$ where Q_0 and x_0 are free parameters) indicates the saturation limit where the DGLAP and GLR-MQ terms in the non-linear equation become equal and is usually defined as [9,37]

$$\frac{\partial xg(x, Q^2)}{\partial \ln Q^2} \Big|_{Q^2=Q_s^2(x)} = 0 \text{ and } \frac{\partial xS(x, Q^2)}{\partial \ln Q^2} \Big|_{Q^2=Q_s^2(x)} = 0,$$

where $xS(x, Q^2)$ is the sea quark distribution. At $Q^2 > Q_s^2(x)$ the linear DGLAP part in the region of applicability of the DGLAP+GLRMQ is dominant and at $Q^2 < Q_s^2(x)$ the GLRMQ terms dominant as all non-linear terms become important, or equivalently

$$\frac{\text{non-linear terms}}{\text{linear terms}} \Big|_{Q^2=Q_s^2(x)} = 1.$$

This balances the linear and non-linear splitting effects at $Q^2 = Q_s^2(x)$.

This paper is organized as follows. In the next section the theoretical formalism is presented, including the non-linear evolution and the parametrization models. In section 3, we present a detailed numerical analysis and our main results. We then confront these results with the CDM bounds and the HERA data at low values of Q^2 . In the last section we summarize our main conclusions and remarks.

2. Theoretical formalism

The structure function F_2 is expressed through the quark and gluon densities as

$$F_2(x, Q^2) = B_{2,s}(x, Q^2) \otimes F_2^s(x, Q^2) + \langle e^2 \rangle B_{2,g}(x, Q^2) \otimes xg(x, Q^2), \quad (3)$$

where $B_{2,a}(a = s, g)$ are the common Wilson coefficient functions and the symbol \otimes denotes a convolution according to the usual prescription, $f(x) \otimes g(x) = \int_x^1 \frac{dy}{y} f(y) g(\frac{x}{y})$. Here using the fact that the non-singlet contribution can be ignored safely at low values of x . The

DGLAP evolution equations can be written as

$$\begin{aligned}\frac{\partial F_2^s(x, Q^2)}{\partial \ln Q^2} &= -\frac{a_s(Q^2)}{2}[(P_{ss}^{(0)}(x) + a_s(Q^2)\tilde{P}_{ss}^{(1)}(x) \\ &\quad + \dots) \otimes F_2^s(x, Q^2) + \langle e^2 \rangle (P_{sg}^{(0)}(x) \\ &\quad + a_s(Q^2)\tilde{P}_{sg}^{(1)}(x) + \dots) \otimes xg(x, Q^2)], \\ \frac{\partial xg(x, Q^2)}{\partial \ln Q^2} &= -\frac{a_s(Q^2)}{2}[\langle e^2 \rangle^{-1} (P_{gs}^{(0)}(x) + a_s(Q^2) \\ &\quad \times \tilde{P}_{gs}^{(1)}(x) + \dots) \otimes F_2^s(x, Q^2) \\ &\quad + (P_{gg}^{(0)}(x) + a_s(Q^2)\tilde{P}_{gg}^{(1)}(x) \\ &\quad + \dots) \otimes xg(x, Q^2)],\end{aligned}\quad (4)$$

where

$$\tilde{P}_{ab}^{(n)}(x) = P_{ab}^{(n)}(x) + [B_{2,s} + B_{2,g} + \dots] \otimes P_{ab}^{(0)}(x) + \dots$$

The quantities \tilde{P}_{ab} 's are expressed via the known splitting and Wilson coefficient functions in literatures [38,39] and P_{ab} are the splitting functions in [40]. The running coupling in the high-loop corrections of the above equation is expressed entirely thorough the variable $a_s(Q^2)$ where $a_s(Q^2) = \frac{\alpha_s(Q^2)}{4\pi}$. Also $\langle e^k \rangle$ is the average of the charge e^k for the active quark flavors, $\langle e^k \rangle = n_f^{-1} \sum_{i=1}^{n_f} e_i^k$.

In perturbative QCD, the longitudinal structure function in terms of the coefficient functions at small x is given by [41]

$$F_L(x, Q^2) = C_{L,q}(\alpha_s, x) \otimes F_2^s(x, Q^2) + \langle e^2 \rangle C_{L,g}(\alpha_s, x) \otimes xg(x, Q^2), \quad (5)$$

where the coefficient functions can be written as [42]

$$C_{L,a}(\alpha_s, x) = \sum_{n=1} a_s(Q^2)^n c_{L,a}^n(x), \quad (6)$$

and n is the order in the running coupling.

The proton structure function parametrized in Refs.[7] and [8] with a global fit function to the ZEUS data and to combined HERA data respectively for $F_2(x, Q^2)$ in a wide range of Q^2 at $x < 0.1$, as

$$\begin{aligned}F_2(x, Q^2) &= (1-x) \left[\frac{F_P}{1-x_P} + A(Q^2) \ln\left(\frac{x_P}{x} \frac{1-x}{1-x_P}\right) \right. \\ &\quad \left. + B(Q^2) \ln^2\left(\frac{x_P}{x} \frac{1-x}{1-x_P}\right) \right].\end{aligned}\quad (7)$$

Here x_P is an approximate fixed point observed in the data where curves of $F_2^p(x, Q^2)$ for different Q^2 cross. Also

$$A(Q^2) = a_0 + a_1 \ln Q^2 + a_2 \ln^2 Q^2,$$

and

$$B(Q^2) = b_0 + b_1 \ln Q^2 + b_2 \ln^2 Q^2.$$

The fitted parameters are tabulated in Table I. In terms of the measured structure function $F_2(x, Q^2)$ (i.e., Eq.(7)), the gluon distribution function is determined due to the Laplace transform method in Ref.[7]. In the case of four massless quarks, the gluon distribution function is obtained with an expression quadratic in both $\ln Q^2$ and $\ln(1/x)$ for $0 < x \leq 0.06$ as

$$\begin{aligned}G(x, Q^2) &= \frac{3}{5}[-2.94 - 0.359 \ln Q^2 - 0.101 \ln^2 Q^2 \\ &\quad + (0.594 - 0.0792 \ln Q^2 - 0.000578 \ln^2 Q^2) \\ &\quad \times \ln(1/x) + (0.168 + 0.138 \ln Q^2 \\ &\quad + 0.0169 \ln^2 Q^2) \ln^2(1/x)].\end{aligned}\quad (8)$$

In Refs.[43,44] the behavior of the longitudinal structure function due to the Mellin transform and Regge theory have been considered respectively. The authors in Ref.[43] obtained analytical relations for the longitudinal structure function at LO and NLO approximations in terms of the effective parameters of the parametrization of the proton structure function. With respect to the Mellin transform method, the LO and NLO longitudinal structure functions are obtained at low x by the following forms

$$F_L^{\text{LO}}(x, Q^2) = (1-x)^n \sum_{m=0}^2 C_m(Q^2) L^m, \quad (9)$$

where L 's are the logarithmic terms, and

$$\begin{aligned}F_L^{\text{NLO}}(x, Q^2) &= \frac{1}{[1 + \frac{1}{3}a_s(Q^2)L_C(\tilde{\delta}_{sg}^{(1)} - \tilde{R}_{L,g}^{(1)})]} \left\{ \right. \\ &\quad [1 - a_s(Q^2)(\tilde{\delta}_{sg}^{(1)} - \tilde{R}_{L,g}^{(1)})] F_L^{\text{LO}}(x, Q^2) \\ &\quad \left. - a_s^2(Q^2) [\frac{1}{3}\tilde{B}_{L,s}^{(1)}L_A + \tilde{B}_{L,s}^{(1)}] F_2(x, Q^2) \right\}.\end{aligned}\quad (10)$$

The coefficient functions at LO and NLO approximations are summarized in Appendix A and also the effective parameters are defined in Table II. Therefore the parametrization of $\sigma_r(x, Q^2)$ in terms of the Froissart-bounded parametrizations of $F_2(x, Q^2)$ and $F_L(x, Q^2)$ at LO and NLO approximations read as

$$\begin{aligned}\sigma_r^{(n)}(x, Q^2) &= D(Q^2)(1-x)^\nu \sum_{m=0}^2 A_m(Q^2) L^m \\ &\quad - f(y) F_L^{(n)}(x, Q^2)\end{aligned}\quad (11)$$

where $f(y) = y^2/Y_+$, $Y_+ = 1 + (1-y)^2$ and $y = Q^2/sx$. The first and second order results (i.e., $n = 1$ and 2) shows the LO ($n = 1$) and NLO ($n = 2$) longitudinal coefficient functions. Recently, the non-linear modification of the evolution of the gluon density at small x is considered in the leading order of perturbation

theory in Ref.[45]. In Ref.[17] the important role of absorptive effects and power corrections in low x DGLAP evolution are considered. These effects flat the behavior of the low x gluon density which arises from the freezing of α_s at low Q^2 values. In the following the extraction of the non-linear corrections provides means for determining distribution functions and reduced cross sections at low x and low Q^2 values with respect to the phenomenological assumptions. In the following, these non-linear modifications will be applied to the distribution functions at high-order corrections.

3. Results and discussions

Effects of non-linear gluon corrections are obtained by solving the GLR-MQ equation (i.e., Eq.(1)) in standard form

$$\frac{\partial G(x, Q^2)}{\partial \ln Q^2} = \frac{\partial G(x, Q^2)}{\partial \ln Q^2} \Big|_{DGLAP} - \frac{81}{16} \frac{\alpha_s^2(Q^2)}{\mathcal{R}^2 Q^2} \int_{\chi}^1 \frac{dz}{z} G^2\left(\frac{x}{z}, Q^2\right). \quad (12)$$

By solving the above equation (i.e., Eq.(12)), the non-linear corrections to the gluon distribution function (i.e., $G^{\text{NLC}}(x, Q^2)$) is obtained by the following form as

$$G^{\text{NLC}}(x, Q^2) = G^{\text{NLC}}(x, Q_0^2) + [G(x, Q^2) - G(x, Q_0^2)] - \int_{Q_0^2}^{Q^2} \frac{81}{16} \frac{\alpha_s^2(Q^2)}{\mathcal{R}^2 Q^2} \int_{\chi}^1 \frac{dz}{z} G^2\left(\frac{x}{z}, Q^2\right) d \ln Q^2 \quad (13)$$

where $G(x, Q^2)$ and $G(x, Q_0^2)$ are the unshadowed gluon distributions and obtained from the solutions to standard DGLAP equations which determined through a fit to HERA data (according to Eq.(8)). We note that at $x \geq x_0 (= 10^{-2})$ the non-linear corrections are negligible. At the initial scale Q_0^2 , the low x behavior of the non-linear gluon distribution is assumed to be [37]

$$G^{\text{NLC}}(x, Q_0^2) = G(x, Q_0^2) \left\{ 1 + \frac{27\pi\alpha_s(Q_0^2)}{16\mathcal{R}^2 Q_0^2} \theta(x_0 - x) \times [G(x, Q_0^2) - G(x_0, Q_0^2)] \right\}^{-1}. \quad (14)$$

Indeed authors in Ref.[37] impose shadowing corrections by modifying gluon density for $x < x_0$, where the leading shadowing approximation g_{sat} is the value of the gluon which would saturate the unitarity limit as $xg_{\text{sat}}(x, Q^2) = \frac{16\mathcal{R}^2 Q^2}{27\pi\alpha_s(Q^2)}$. The non-linear corrections to the longitudinal structure function is defined as

$$F_L^{\text{NLC}}(x, Q^2) = C_{L,q}(\alpha_s, x) \otimes F_2^s(x, Q^2) + \langle e^2 \rangle C_{L,g}(\alpha_s, x) \otimes G^{\text{NLC}}(x, Q^2), \quad (15)$$

Therefore the non-linear corrections to the reduced cross section is defined by

$$\sigma_r^{\text{NLC}}(x, Q^2) = F_2(x, Q^2) - f(y) F_L^{\text{NLC}}(x, Q^2) \quad (16)$$

The analysis is performed in the ranges of $10^{-5} \leq x \leq 10^{-2}$ and $1 \leq Q^2 \leq 1000 \text{ GeV}^2$. The computed results of the non-linear distribution functions are compared with the parametrization methods [7,43] and the experimental data [46-48].

In Fig.1, the computed results of the non-linear gluon distribution function are compared with the linear parametrization model [7]. This behavior is considered at $x < 10^{-2}$ for $Q^2 = 10, 30, 50$ and 100 GeV^2 in the hot-spot point where the value of this parameter is defined to be $R = 2 \text{ GeV}^{-1}$ in this paper. In Fig.2 we show the non-linear results at an input $Q^2 = 1.9 \text{ GeV}^2$ in comparison with the absorptive corrections at low x and the power corrections at low Q^2 values in Ref.[17]. As can be observed in Fig.2, the behavior of the gluon distribution is flat due to the freezing of α_s in comparison with the non-linear behavior due to the parametrization model. The confinement effect is expected to modify the running of the QCD coupling $\alpha_s(Q^2)$ to $\alpha_s(Q^2 + \mu_0^2)$ where μ_0 is the factorization scale. The results compared with $\mu_0^2 = 0$, corresponding to no effects of confinement, and with those obtained for $\mu_0^2 = 1 \text{ GeV}^2$ in Ref.[17].

In Fig.3 we make a critical study of the ratio G/F_2 proposed in the last years [49,50] at linear and non-linear corrections, which is frequently used to extract the gluon distribution from the proton structure function. The ratio G/F_2 is obtained at $Q^2 = 5, 100$ and 1000 GeV^2 at low values of x with respect to the non-linear behavior of the gluon distribution function due to the parametrization model. As can be observed in Fig. 3, this ratio in a wide range of x and Q^2 values is dependent not only to Q^2 , but also to x at linear and non-linear corrections. A purely Q^2 or x independence of the ratio were found in Refs.[50] to be not global in general as compared with our results with respect to the parametrization model.

H1 Collaboration [46] shows that measurement of the derivative $(\partial F_2 / \partial \ln Q^2)_x$ has long been recognised as a powerful constraint of the gluon density and running coupling. For each bin of x , H1 Collaboration [46] shows that these derivatives described by the function $b(x) + 2c(x) \ln Q^2$, while in parametrization model it described in terms of $\ln Q^2$ and $\ln x$ [7]. In Fig.4 the linear and non-linear behavior of the quantity $(\partial F_2 / \partial \ln Q^2)_x$ are considered and compared with the H1 Collaboration data [46] as accompanied with total errors. The non-linear correction to the derivative $(\partial F_2 / \partial \ln Q^2)_x$ is performed due to the non-linear gluon interaction effects in Eq.(2). The non-linear behavior of the quantity is comparable with the H1 Collaboration data in comparison with the linear behavior at low x . The non-linear effects can be tested at a superior statistical accuracy attainable at the LHeC and FCC-he.

In the following, we present the non-linear results that have been obtained for the longitudinal structure function $F_L(x, Q^2)$, the ratio $F_L(x, Q^2)/F_2(x, Q^2)$ and the reduced cross section $\sigma_r(x, Q^2)$ from data mediated by the parametrization of $F_2(x, Q^2)$. The results for the longitudinal structure function are presented in Fig.5 and compared with the H1 data [48] as accompanied with total errors where the average x for each Q^2 is provided on the upper scale of the figure. We use the non-linear longitudinal structure function at NLO and NNLO approximations where effects of the non-linear corrections to the gluon distribution are taken into account. Non-linear results at NLO and NNLO approximations are compared to the parametrization of F_L at NLO approximation [43] and also CT18 [4] at NNLO approximation (CT18 results have been performed at fixed value of the invariant mass W as $W = 230$ GeV). In Fig.6 the non-linear correction to the ratio F_L/F_2 at NNLO approximation is calculated and presented. In this figure the ratio of the structure functions are compared with the H1 Collaboration data [48]. The error bars of the ratio F_L/F_2 are determined by $\Delta(\frac{F_L}{F_2}) = \frac{F_L}{F_2} \sqrt{(\frac{\Delta F_L}{F_L})^2 + (\frac{\Delta F_2}{F_2})^2}$, where ΔF_L and ΔF_2 are collected from the H1 experimental data in Ref.[48]. The non-linear results obtained of the ratio F_L/F_2 are comparable to the results of the color dipole model bounds [51] and experimental data [48]. This comparisons are very good at low- and high- Q^2 values, even compared to the parametrization model [7,43]. The good agreement between the non-linear correction at NNLO analysis and the experimental data indicates that these results have a bound asymptotic behavior and they are compatible with the color dipole model bounds. As can be observed in Fig. 6, the ratio has little dependence on the x -evolution.

In Fig.7 we present the non-linear corrections to the reduced cross section at NNLO approximation at $Q^2 = 8.5$ and 18 GeV². As can be seen in this figure, one can conclude that the non-linear corrections to the results essentially improve the good agreement with data in comparison with the parametrization model at low Q^2 . HERA combined data [47] are taken with center of mass energy $\sqrt{s} = 318$ GeV as accompanied with total errors. These low- x predictions are fully compatible with the H1 data presented in [47]. The non-linear corrections are depicted and compared with the linear parametrization models in this figure. Consequently, the non-linear corrections make it possible to perform the high-order corrections to the ultra-high-energy processes.

5. Summary

In conclusion, we have studied the effects of adding the non-linear corrections to the distribution functions for transition from the linear to non-linear regions. We use the parametrization of $F_2(x, Q^2)$ and $F_L(x, Q^2)$ as baselines. The non-linear corrections to the distribution functions, to the derivative of the proton structure function, to the ratio of structure functions, and to the reduced cross sections at NNLO approximation are considered. Comparing these quantities with the parametrization and the color dipole models indicates that the non-linear corrections are enriched by the behavior of distribution functions at low Q^2 . The transition of the ratio F_L/F_2 from the linear to the non-linear behavior is considered and shows that it is in good agreement with the color dipole model bounds not only at high- Q^2 , but also at low- Q^2 values. Comparison of the reduced cross sections with respect to the non-linear corrections with HERA data at low and moderate Q^2 values shows that this transition has been performed with good accuracy in comparison with the HERA combined data. It has been found that at low and moderated Q^2 , NNLO results are corresponding to the experimental data and parametrization methods. The non-linear method can be used in low- x and low- Q^2 at the LHeC project.

Appendix A

The coefficient functions read as

$$\begin{aligned} C_2 &= \hat{A}_2 + \frac{8}{3}a_s(Q^2)DA_2 \\ C_1 &= \hat{A}_1 + \frac{1}{2}\hat{A}_2 + \frac{8}{3}a_s(Q^2)D[A_1 + (4\zeta_2 - \frac{7}{2})A_2] \\ C_0 &= \hat{A}_0 + \frac{1}{4}\hat{A}_2 - \frac{7}{8}\hat{A}_2 + \frac{8}{3}a_s(Q^2)D[A_0 + (2\zeta_2 - \frac{7}{4})A_1 \\ &\quad + (\zeta_2 - 4\zeta_3 - \frac{17}{8})A_2], \end{aligned} \quad (17)$$

$$\begin{aligned} \hat{A}_2 &= \tilde{A}_2 \\ \hat{A}_1 &= \tilde{A}_1 + 2DA_2 \frac{\mu^2}{\mu^2 + Q^2} \\ \hat{A}_0 &= \tilde{A}_0 + DA_1 \frac{\mu^2}{\mu^2 + Q^2} \\ \tilde{A}_i &= \tilde{D}A_i + D\bar{A}_i \frac{Q^2}{Q^2 + \mu^2} \\ \tilde{D} &= \frac{M^2 Q^2 [(2 - \lambda)Q^2 + \lambda M^2]}{[Q^2 + M^2]^3} \\ \bar{A}_m &= a_{m1} + 2a_{m2}L_2, \quad a_{02} = 0. \end{aligned} \quad (18)$$

and

$$\begin{aligned}
\widehat{B}_{L,s}^{(1)} &= 8C_F \left[\frac{25}{9}n_f - \frac{449}{72}C_F + (2C_F - C_A) \right. \\
&\quad \left. (\zeta_3 + 2\zeta_2 - \frac{59}{72}) \right] \\
\overline{B}_{L,s}^{(1)} &= \frac{20}{3}C_F(3C_A - 2n_f) \\
\widehat{\delta}_{sg}^{(1)} &= \frac{26}{3}C_A \\
\overline{\delta}_{sg}^{(1)} &= 3C_F - \frac{347}{18}C_A \\
\widehat{R}_{L,g}^{(1)} &= -\frac{4}{3}C_A \\
\overline{R}_{L,g}^{(1)} &= -5C_F - \frac{4}{9}C_A \\
L_A &= L + \frac{A_1}{2A_2} \\
L_C &= L + \frac{C_1}{2C_2} \\
L &= \ln(1/x) + L_1 \\
L_1 &= \ln \frac{Q^2}{Q^2 + \mu^2} \\
L_2 &= \ln \frac{Q^2 + \mu^2}{\mu^2} \\
A_i(Q^2) &= \sum_{k=0}^2 a_{ik} L_2^k, \quad (i = 1, 2) \\
A_0 &= a_{00} + a_{01} L_2 \\
D &= \frac{Q^2(Q^2 + \lambda M^2)}{(Q^2 + M^2)^2}.
\end{aligned} \tag{19}$$

TABLE I: The effective parameters at low x for $0.11 \text{ GeV}^2 < Q^2 < 1200 \text{ GeV}^2$ are defined by the following values.

parameters	value
a_0	$-7.828 \times 10^{-2} \pm 5.19 \times 10^{-3}$
a_1	$2.248 \times 10^{-2} \pm 1.47 \times 10^{-3}$
a_2	$2.301 \times 10^{-4} \pm 4.88 \times 10^{-4}$
b_0	$1.313 \times 10^{-2} \pm 6.99 \times 10^{-4}$
b_1	$4.736 \times 10^{-3} \pm 2.98 \times 10^{-4}$
b_2	$1.064 \times 10^{-3} \pm 3.88 \times 10^{-5}$
x_P	0.0494 ± 0.0039
F_P	0.503 ± 0.012
χ_{min}^2	193.19

TABLE II: The effective parameters used in appendix A with respect to Eqs.(9) and (10) in Ref.[43].

parameters	value
a_{00}	$2.550 \times 10^{-1} \pm 1.600 \times 10^{-2}$
a_{01}	$1.475 \times 10^{-1} \pm 3.025 \times 10^{-2}$
a_{10}	$8.205 \times 10^{-4} \pm 4.62 \times 10^{-4}$
a_{11}	$-5.148 \times 10^{-2} \pm 8.19 \times 10^{-3}$
a_{12}	$-4.725 \times 10^{-3} \pm 1.01 \times 10^{-3}$
a_{20}	$2.217 \times 10^{-3} \pm 1.42 \times 10^{-4}$
a_{21}	$1.244 \times 10^{-2} \pm 8.56 \times 10^{-4}$
a_{22}	$5.958 \times 10^{-4} \pm 2.32 \times 10^{-4}$

ACKNOWLEDGMENTS

We are grateful to the Razi University for financial support of this project. G.R.Boroun was especially grateful to A.V.Kotikov for carefully reading the paper and for critical notes.

REFERENCES

1. L.N. Lipatov, Sov. J. Nucl. Phys.**20**, 94 (1975); V.N. Gribov, L.N. Lipatov, Sov. J. Nucl. Phys.**15**, 438 (1972); G. Altarelli, G. Parisi, Nucl. Phys. B**126**, 298 (1977); Yu.L. Dokshitzer, Sov. Phys. JETP **46**, 641 (1977).
2. A.D.Martin, R.G.Roberts, W.J.Stirling and R.S.Thorne, Eur.Phys.J.C**23**, 73(2002); Phys.Lett.B **531**, 216 (2002).
3. CTEQ Collaboration, J.Pumplin et al., J.High Energ.Phys.**07**, 012 (2002).
4. Tie-Jiun Hou et al., Phys.Rev.D **103**, 014013 (2021).
5. H1 Collaboration, C.Adloff et al., Eur.Phys.J.C **12**, 375 (2000).
6. M. Froissart, Phys.Rev.**123**, 1053 (1961).
7. M. M. Block and L. Durand, arXiv [hep-ph]: 0902.0372 (2009).
8. M. M. Block, L. Durand and P. Ha, Phys. Rev.D **89**, 094027 (2014).
9. R. Fiorea et al., Phys.Rev.D **71**, 033002 (2005); R.Fiorea et al., Phys.Rev.D **73**, 053012 (2006).
10. LHeC Collaboration and FCC-he Study Group , P.Agostini et al., CERN-ACC-Note-2020-0002, arXiv:2007.14491 [hep-ex] (2020).
11. M.Klein, Annalen Phys.**528**, 138 (2016); M.Klein, arXiv [hep-ph]:1802.04317.
12. N.Armesto et al., Phys.Rev.D **100**, 074022 (2019).

13. K.J.Eskola et al., Nucl.Phys.B **660**, 211 (2003); K.J.Eskola et al., arXiv: hep-ph/0302185 (2003); M.A.Kimber, J.Kwiecinski and A.D.Martin, Phys.Lett.B **508**, 58 (2001).
14. K.Prytz, Eur.Phys.J.C **22**, 317 (2001).
15. G.Ingelman and K.Prytz, Z.Phys.C **58**, 285 (1993).
16. B.Rezaei and G.R.Boroun, Phys.Lett.B **692**, 247 (2010).
17. M.R.Pelicer et al., Eur.Phys.J.C **79**, 9 (2019).
18. G.R.Boroun, Eur.Phys.J.A **43**, 335 (2010).
19. M.Devee and J.K.Sarma, Eur.Phys.J.C **74**, 2751 (2014); arXiv [hep-ph]: 1808.01586 (2018); Nucl.Phys.B **885**, 571 (2014); M.Devee, arXiv [hep-ph]: 1808.00899 (2018).
20. B.Rezaei and G.R.Boroun, Phys.Rev.C **101**, 045202 (2020).
21. M.Lalung, P.Phukan and J.K.Sarma, Int.J.Theor.Phys.**56**, 11(2017); Nucl.Phys.A **992**, 12615 (2019); arXiv [hep-ph]:1801.06360(2019).
22. G.R.Boroun, Phys.Rev.C **97**, 015206 (2018).
23. H.Khanpour, Phys.Rev.D **99**, 054007 (2019).
24. G.R.Boroun and S.Zarrin, Eur.Phys.J.Plus **128**, 119 (2013).
25. P.Phukan, M.Lalung and J.K.Sarma, Nucl.Phys.A **968**, 275 (2017).
26. B.Rezaei and G.R.Boroun, Eur.Phys.J.A **55**, 66 (2019).
27. R.Wang and X.Chen, Chinese Phys.C **41**, 053103 (2017).
28. G.R.Boroun and B.Rezaei, Nucl.Phys.A **1006**, 122062 (2021).
29. A.Kovner and Urs A.Wiedemann, Phys.Rev.D **66**, 051502 (2002).
30. G.R.Boroun, JETP Letters **114**, 1 (2021).
31. J.Gao, L.Harland-Lang and J.Rojo, Phys.Rept.**742**, 1 (2018).
32. I.I.Balitsky and A.V.Belitsky, Nucl.Phys.B **629**, 290 (2002).
33. A.M.Stasto, Acta Phys.Polon.B **33**, 1571(2002).
34. R.D.Ball et al., Eur.Phys.J.C **78**, 321 (2018); xFitter Collaboration, H.Abdolmaleki et al., arXiv:1802.00064.
35. J.Bartels and E.Levin, Nucl.Phys.B **387**, 617 (1992).
36. L.V.Gribov, E.M.Levin and M.G.Ryskin, Phys.Rept.**100**, 1 (1983); A.H.Mueller and J.w.Qiu, Nucl.Phys.B **268**, 427 (1986).
37. J.Kwiecinski et al., Phys.Rev.D **42**, 3645 (1990).
38. J. Blumlein, V. Ravindran and W. van Neerven, Nucl. Phys. B **586**, 349 (2000); S.Catani and F.Hautmann, Nucl.Phys.B **427**, 475 (1994).
39. D.I.Kazakov and A.V.Kotikov, Phys.Lett.B **291**, 171 (1992); E.B.Zijlstra and W.L.van Neerven, Nucl.Phys.B **383**, 525 (1992).
40. W.L. van Neerven, A.Vogt, Phys.Lett.B **490**, 111 (2000); A.Vogt, S.Moch, J.A.M.Vermaseren, Nucl.Phys.B **691**, 129 (2004).
41. G.Altarelli and G.Martinelli, Phys.Lett.B **76**, 89 (1978).
42. S.Moch, J.A.M.Vermaseren, A.Vogt, Phys.Lett.B **606**, 123 (2005).
43. L.P.Kaptari et al., Phys.Rev.D**99**, 096019 (2019); L.P.Kaptari et al., JETP Lett.**109**, 281 (2019)
44. B.Rezaei and G.R.Boroun, Eur.Phys.J.A **56**, 262 (2020).
45. A.V.Kotikov, JETP Lett.**111**, 67 (2020).
46. H1 Collaboration, C.Adloff et al., Eur.Phys.J.C **21**, 33 (2001).
47. H1 Collaboration and ZEUS Collaboration, H. Abramowicz et al., Eur. Phys. J. C **75**, 580 (2015).
48. H1 Collaboration, V. Andreev et al., Eur. Phys. J. C **74**, 2814 (2014).
49. G.R.Boroun, Eur.Phys.J.A **50**, 69 (2014).
50. D.K.Choudhury and L.Machahari, arXiv[hep-ph]:2007.00978; L.Machahari and D.K.Choudhury, Eur.Phys.J.A **54**, 69 (2018); J.K.Sarma, K.Choudhury and G.K.Medhi, Phys.Lett.B **403**, 139 (1997); M.Devee, R. Baishya and J.K.Sarma, Eur.Phys.J.C **72**, 2036 (2012).
51. C. Ewerz et al., Phys.lett.B **720**, 181 (2013).

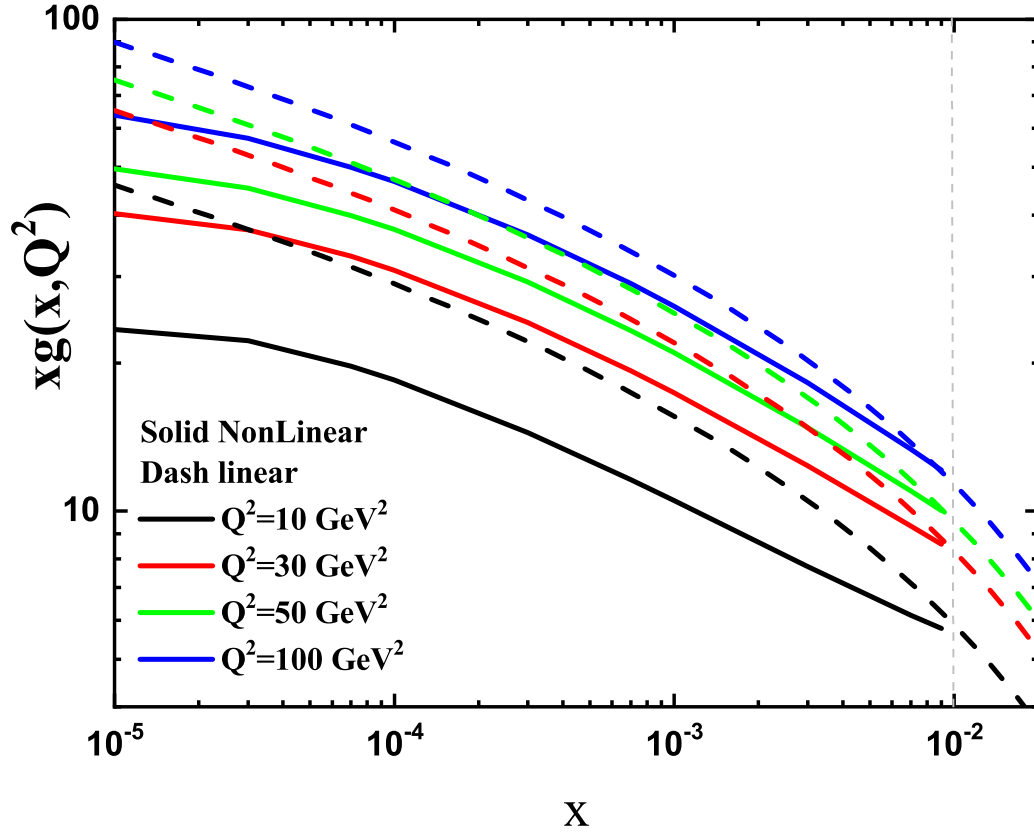


FIG. 1: The linear and non-linear gluon distribution function at $R = 2 \text{ GeV}^{-1}$ for $Q^2 = 10, 30, 50$ and 100 GeV^2 with respect to the parametrization model [7] and GLR-MQ equation [36] respectively.

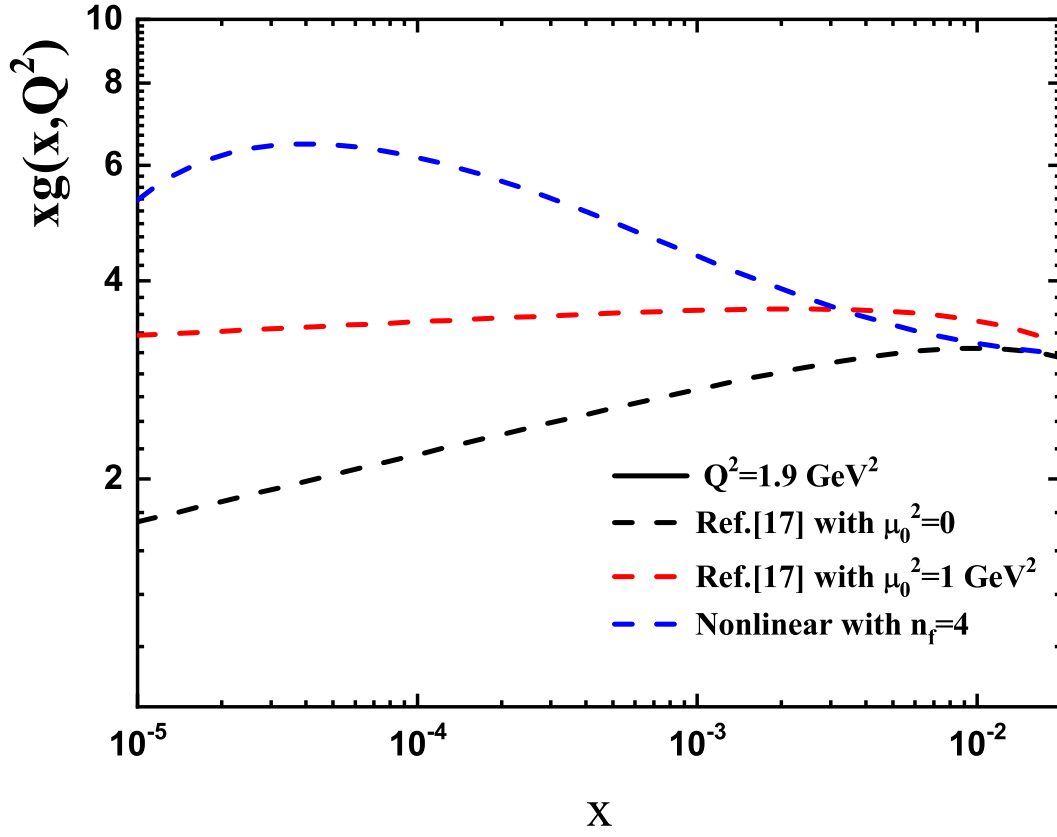


FIG. 2: The non-linear gluon distribution function at $R = 2 \text{ GeV}^{-1}$ and $n_f = 4$ at $Q^2 = 1.9 \text{ GeV}^2$ compared with the power corrections arises from the freezing of the running coupling with $\mu_0^2 = 0$ and 1 GeV^2 [17].

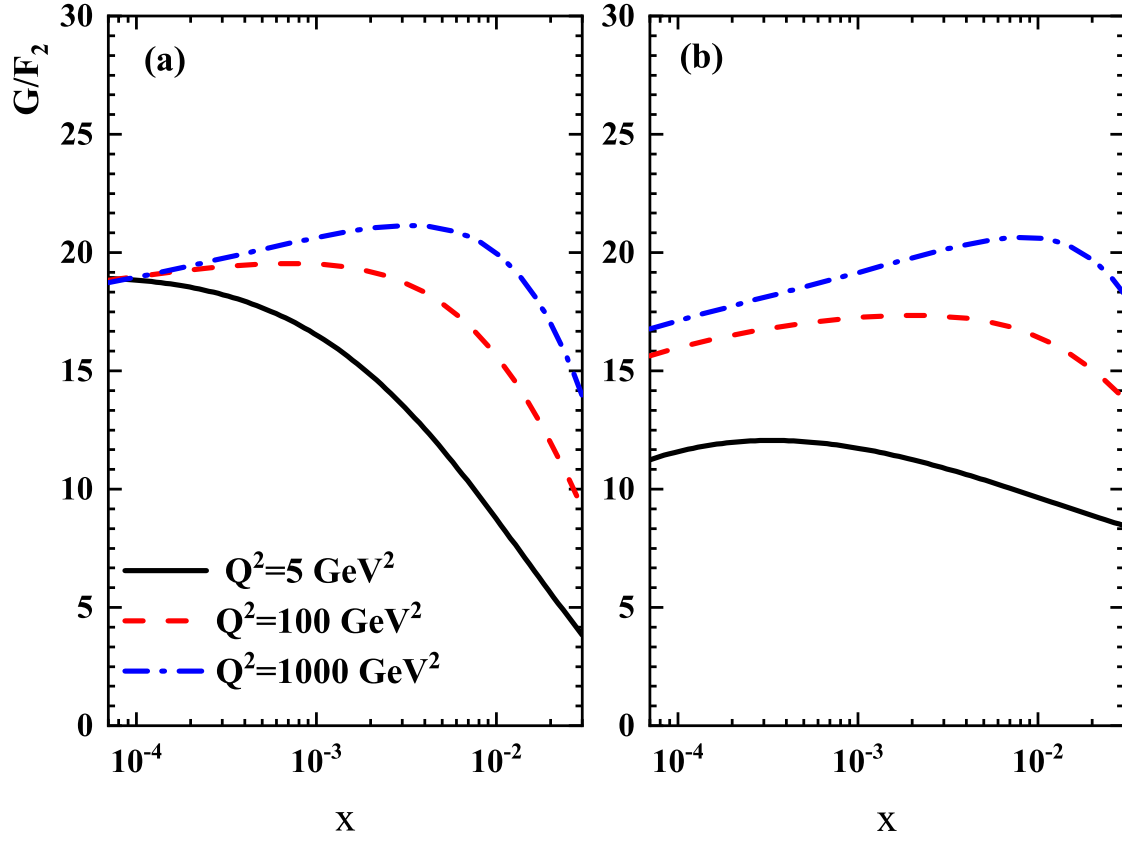


FIG. 3: Results of the ratio $G(x, Q^2)/F_2(x, Q^2)$ at $Q^2 = 5, 100$ and 1000 GeV^2 vs x obtained from (a) the linear and (b) the non-linear parametrization model.

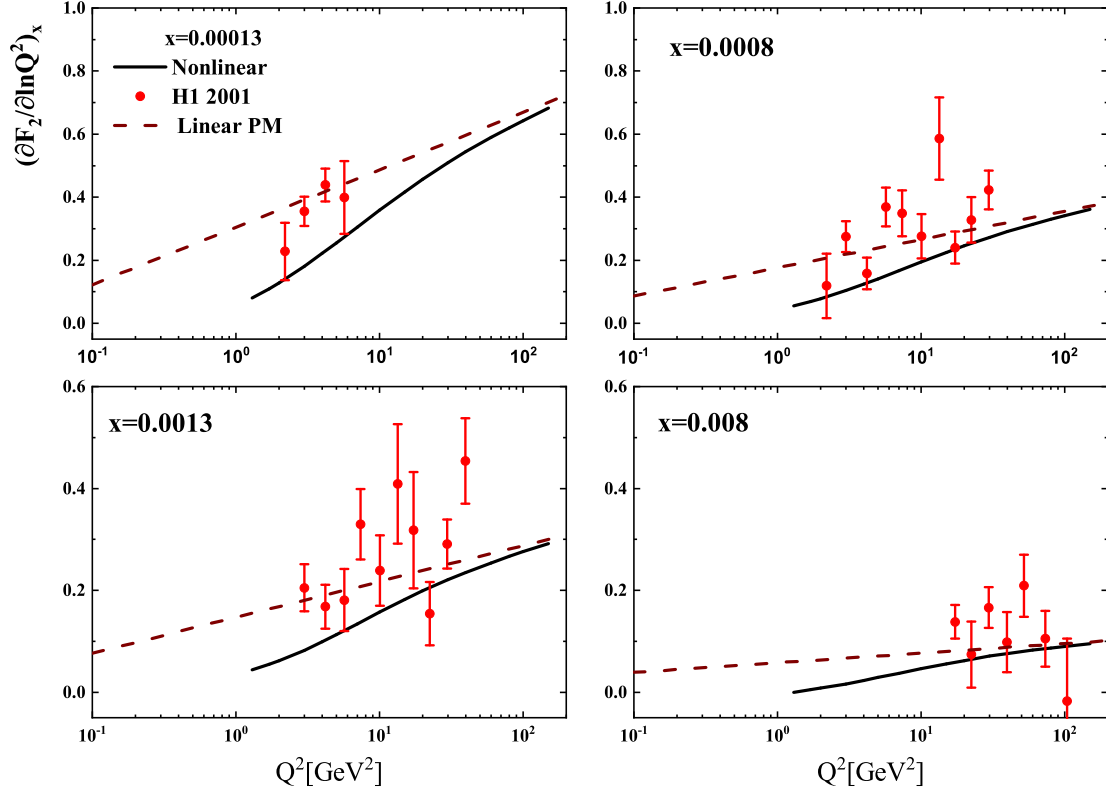


FIG. 4: The derivative $(\partial F_2 / \partial \ln Q^2)_x$ plotted as functions of Q^2 for fixed x compared with the H1 Collaboration data [46] as accompanied with total errors. The linear and non-linear behaviors are obtained from the parametrization model.

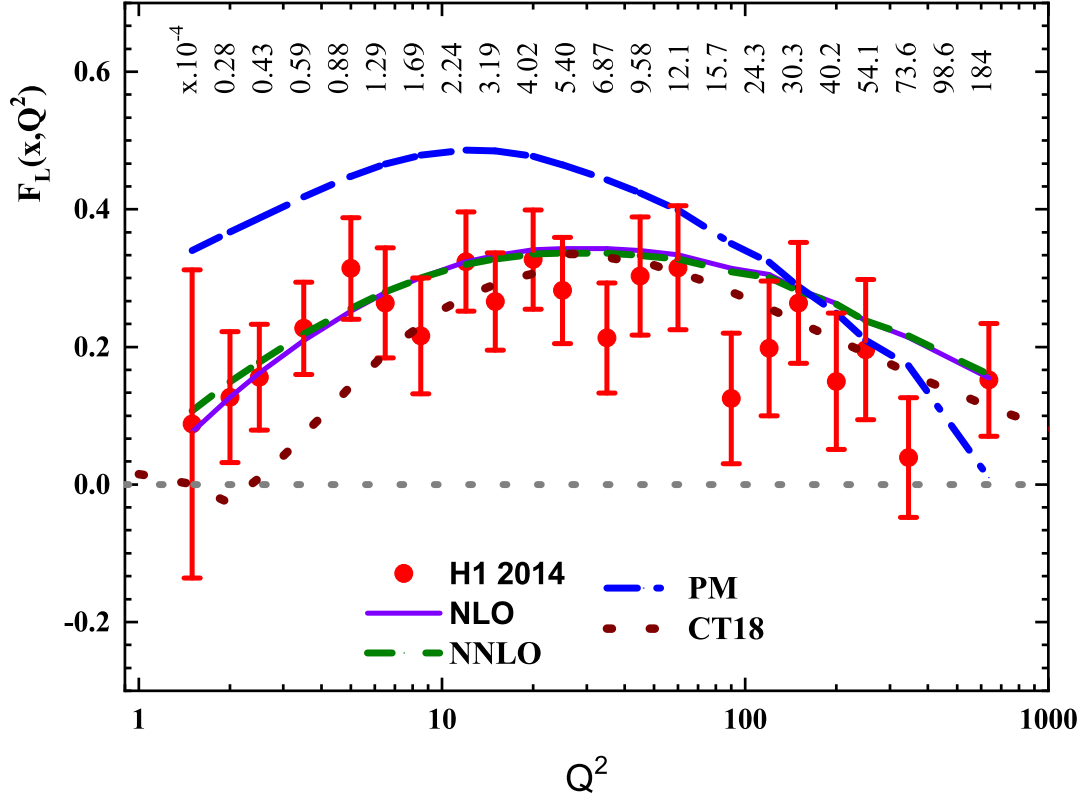


FIG. 5: The non-linear longitudinal structure function F_L at NLO and NNLO approximations averaged over x at different Q^2 . The average value of x for each Q^2 is given above each data point. The non-linear results at NLO (solid) and NNLO (dashed) are compared to the H1 Collaboration data [48] as accompanied with total errors, the parametrization model [43] (dashed-dot) and CT18 [4](dot) at the NNLO approximation at fixed value of the invariant mass $W = 230$ GeV.

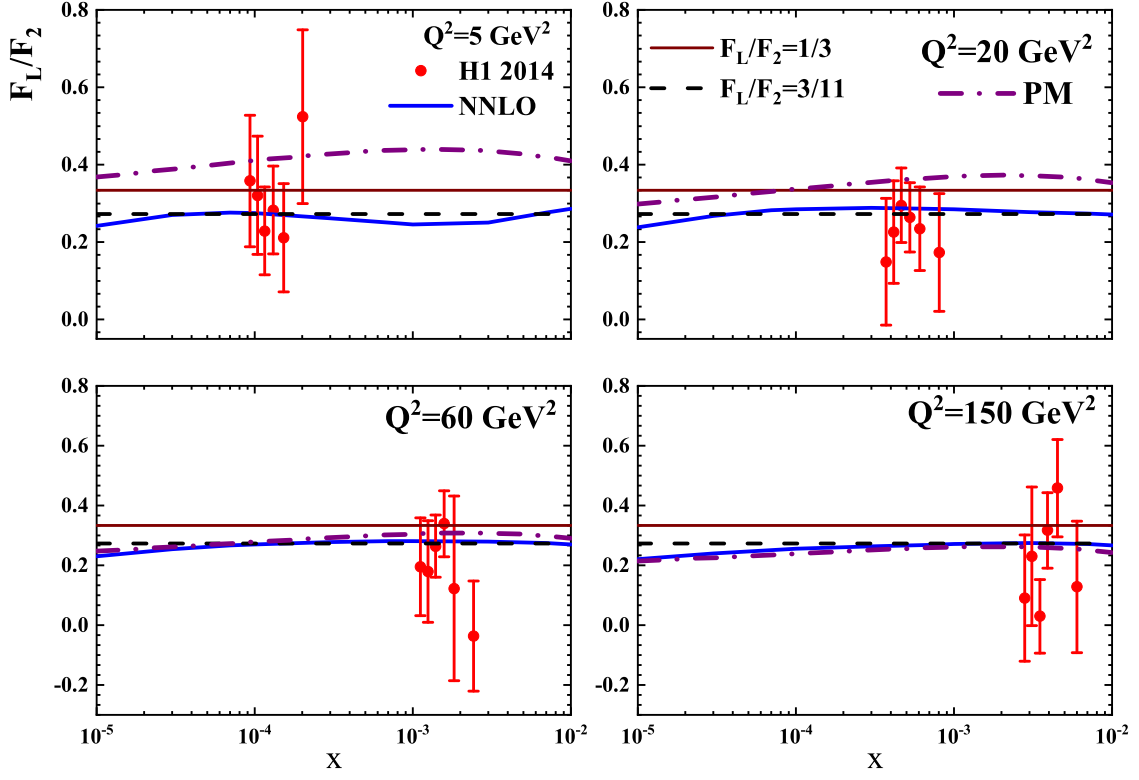


FIG. 6: Results of the ratio F_L/F_2 obtained from the non-linear corrections at NNLO approximation at fixed Q^2 values. The ratio compared with the color dipole picture bounds (i.e., $F_L/F_2 = 1/3$ and $3/11$), H1 Collaboration data [48] as accompanied with total errors, and the parametrization model [7,43].

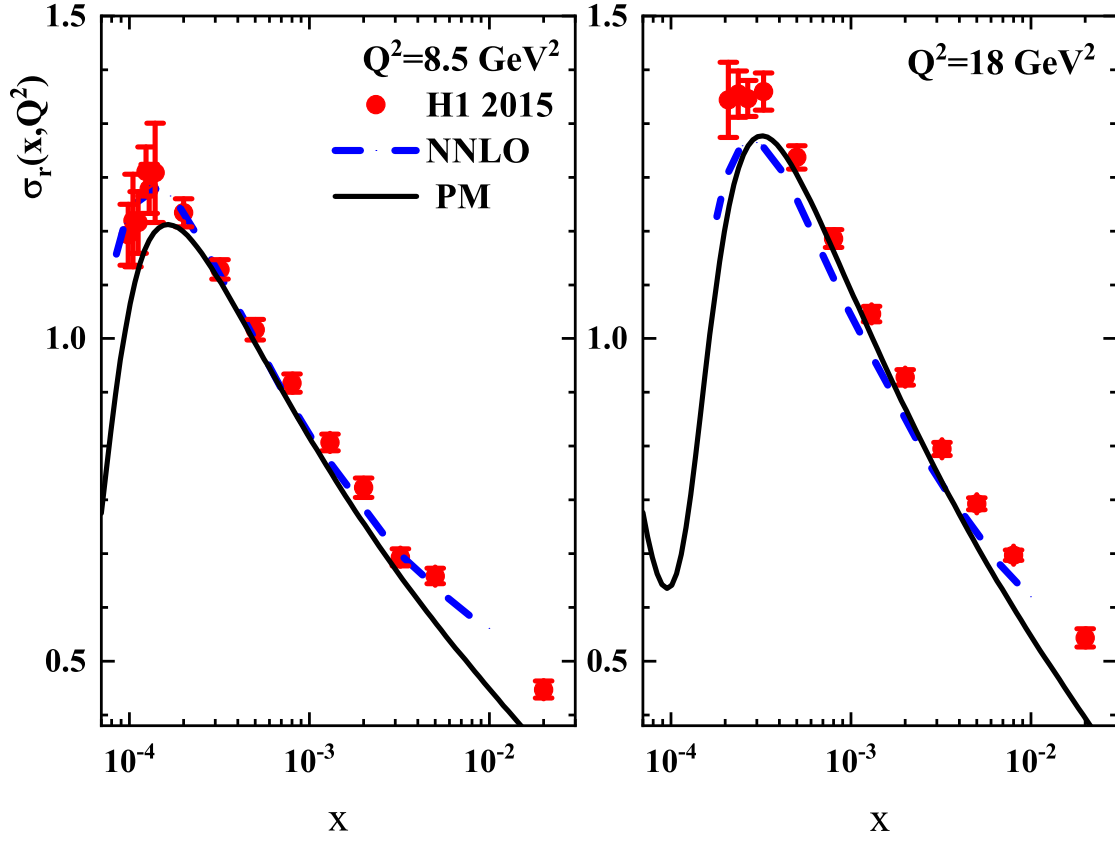


FIG. 7: The NNLO predictions for the reduced DIS cross section at $Q^2 = 8.5$ and 18 GeV^2 available. The H1 data for some representative fixed values of Q^2 are taken from [47] as accompanied with total errors. The non-linear corrections of the reduced cross section at NNLO approximation compared with the parametrization model.